July 2006

The Consensus Mechanics of Cultured Mammalian Cells

Brenton D. Hoffman
University of Pennsylvania

Gladys Massiera
University of Pennsylvania

Kathleen A. Miranda
University of Pennsylvania

John C. Crocker
University of Pennsylvania, jcrocker@seas.upenn.edu

Copyright National Academy of Sciences. Postprint version. Published in *Proceedings of the National Academy of Sciences of the United States of America*, Volume 103, Issue 27, July 2006, pages 10259-10264.
Publisher URL: http://www.pnas.org/cgi/reprint/103/27/10259

The Consensus Mechanics of Cultured Mammalian Cells

Abstract

While understanding cells' responses to mechanical stimuli is seen as increasingly important for understanding cell biology, how to best measure, interpret and model cells' mechanical properties remains unclear. We determine the frequency-dependent shear modulus of cultured mammalian cells using four different methods, both novel and well established. This approach clarifies the effects of cytoskeletal heterogeneity, ATP-dependent processes and cell regional variations on the interpretation of such measurements. Our results clearly indicate two qualitatively similar but distinct mechanical responses, corresponding to the cortical and intracellular networks, each having an unusual, weak power-law form at low frequency. The two frequency dependent responses we observe are remarkably similar to those reported for a variety of cultured mammalian cells measured using different techniques, suggesting it is a useful consensus description. Finally, we discuss possible physical explanations for the observed mechanical response.

Keywords

cell mechanics, cytoskeleton, mechanotransduction, microrheology

The consensus mechanics of cultured mammalian cells

Brenton D. Hoffman[1,*], Gladys Massiera[1,*,†], Kathleen A. Miranda[1], John C. Crocker[1,2]

[1]*Department of Chemical and Biomolecular Engineering, University of Pennsylvania, 220 S. 33rd St., Philadelphia, PA 19104, USA*

[2]*Institute for Medicine and Engineering, University of Pennsylvania, 3340 Smith Walk, Philadelphia, PA 19104, USA*

*These two authors contributed equally to this work.

†Present Address: Laboratoire de Spectrométrie Physique, BP 87, 140 avenue de la Physique 38402 St Martin d'Hères, France.

Classification : Biological Sciences (Biophysics)

Corresponding Author : John C. Crocker, Rm 311A, 220 S. 33rd St, Philadelphia, PA 19104, voice : 215-898-9188, fax : 215-573-2093, email : jcrocker@seas.upenn.edu

Manuscript Info: 24 pages not including 5 figures

Abstract: 137 words

Total Characters (w/spaces): 40,750

Abstract

While understanding cells' responses to mechanical stimuli is seen as increasingly important for understanding cell biology, how to best measure, interpret and model cells' mechanical properties remains unclear. We determine the frequency-dependent shear modulus of cultured mammalian cells using four different methods, both novel and well established. This approach clarifies the effects of cytoskeletal heterogeneity, ATP-dependent processes and cell regional variations on the interpretation of such measurements. Our results clearly indicate two qualitatively similar but distinct mechanical responses, corresponding to the cortical and intracellular networks, each having an unusual, weak power-law form at low frequency. The two frequency dependent responses we observe are remarkably similar to those reported for a variety of cultured mammalian cells measured using different techniques, suggesting it is a useful consensus description. Finally, we discuss possible physical explanations for the observed mechanical response.

The important role of mechanical and physical cues in determining cell behavior is increasingly recognized. Cell shape can modulate cell differentiation (1), while substrate stiffness can affect tissue morphogenesis (2) and myoblast differentiation (3). The mechanisms, however, by which mechanical cues lead to molecular and biochemical responses remain largely undetermined. One approach to studying such mechano-sensing processes is to understand the mechanical properties of cells' constitutive molecules individually. While protein conformation can respond to locally applied, small-scale mechanical signals such as molecular tension (4), how these signals may be combined to sense larger scale mechanical properties remains unclear (5). Ultimately, an integrated physical description of cytoskeletal mechanics will be required to connect these molecular and cellular levels of description.

In soft-matter and polymer physics, the mechanical response and dynamics of supramolecular assemblies are determined using rheology, the study of the frequency-dependent elastic and viscous behavior of deformable materials. Reliably interpreting rheology measurements on living cells, however, has proven notoriously difficult. Only after decades of experimental effort have different cell measurements begun to report comparable responses, while many differences remain (6). The rheology of cells is typically inferred either from deformation in response to an applied force (termed active microrheology) or from the Brownian motion of embedded or attached tracer particles (termed passive microrheology). The results of both approaches depend on theoretical models for the deformation geometry or coupling between the tracer and the cell. Passive methods will also be confounded by any non-Brownian tracer motion such as intracellular trafficking or cell crawling. The comparison of cell mechanics measurements based on different methods is currently confounded by such technical effects, as well as the unknown degree of variability among different cell types.

This paper seeks the consensus mechanical response of living cells by applying a suite of different microrheology techniques to a single cultured mammalian cell type (Figure 1). We apply an original technique that we recently developed, two-point microrheology (TPM) (7), to measure cells' dynamic shear modulus for the first time. While TPM has the advantage that it does not depend on details of the tracer coupling or assumed deformation geometry, providing a uniquely interpretable and quantitative result, it does not probe the cell cortex. For this reason, we also apply an active method using externally-attached magnetic tracers, magnetic twisting cytometry (MTC) (8), and passive methods using the same tracers (either internalized or externally adhered), termed laser tracking microrheology (LTM). When the confounding effects of non-Brownian motion are removed by chemical depletion of intracellular ATP, these four experiments report two distinct frequency dependent shear moduli, which we conclude correspond to the cortical and intracellular cytoskeletal networks. Comparison of our results with the literature shows many earlier measurements made on a variety of cell types matching one or the other of our two mechanical responses, suggesting that our findings may be rather universal.

Both of our observed mechanical responses display weak power-law frequency dependences at low frequencies. While such a power-law form is suggestive of a simple physical origin, the microscopic mechanism causing it is unknown. We will discuss the existing theories and model systems that have been used to describe the cell response and what they imply about cytoskeletal architecture and function.

Results

Our strategy to determine the consensus mechanical response of cells is to use four different cell rheology techniques, sketched in Figure 1, selected to directly address the

technical issues that have confounded the interpretation of earlier measurements: separating the cortical versus intracellular response, uncertainty regarding the connections between tracers and the network, cell heterogeneity and the effect of non-Brownian motion. All four methods were applied to a single cell type, TC7 African green monkey kidney epithelial cells. We performed representative measurements on murine J774A.1 (macrophage-like) and NIH 3T3 (fibroblast) cells as well and found quite similar results.

Mechanical response is quantified with a complex, frequency-dependent shear modulus, $G^*(\omega) = G'(\omega) + iG''(\omega)$, where $G'(\omega)$ and $G''(\omega)$ relate to the elastic and the viscous response, respectively. The shear modulus is determined either directly from tracer motion in response to a sinusoidal driving torque (MTC), or from random tracer displacements $\Delta r(\tau)$ during a lag time interval τ. In LTM, the random motion is quantified by $\langle \Delta r^2(\tau) \rangle$, a mean-squared displacement (MSD). Roughly speaking, the amplitude of the tracers' MSD at lag time τ can be regarded as inversely proportional to the stiffness of its surroundings at frequency, $\omega = 1/\tau$. Unlike LTM, TPM cross-correlates the random Brownian motion of *pairs* of tracers. This correlated motion is equivalent to the motion of a large segment of the network between the two tracers. Essentially, TPM reports the MSD of the network, not the tracers, allowing quantitative measurements even when the tracers' size and connection to the network are not known (9). Moreover, the use of endogenous lipid granules as tracers (6) makes TPM a completely non-invasive method. Finally, the MSDs from both LTM and TPM are converted to $G^*(\omega)$ using the generalized Stokes-Einstein relation (GSER), (see Methods, Eq. 2).

Microrheology of ATP depleted cells and cell-to-cell reproducibility. All three passive methods showed large amplitude motion at long times that decreased markedly

upon ATP depletion using sodium azide and deoxyglucose. This suggests they are corrupted by contributions from non-Brownian sources of tracer motion such as intracellular trafficking or cell crawling. Importantly, our active technique MTC showed no significant change (Fig. 2A) to the frequency dependent response upon ATP depletion. Hypothesizing that ATP depletion does not significantly change our cells' mechanical response, we first discuss the results of all four measurements on ATP depleted cells, and how these results compare with each other and the literature, prior to comparing them to undepleted control cells.

The first issue that must be addressed is tracer-to-tracer and cell-to-cell reproducibility. In general, the amplitude of the rocking motion or MSD reported by all four methods varies dramatically, resembling a log-normal distribution (see Methods) more than a Gaussian one. The log-normal standard deviations (in ATP depleted cells) were Σ=4.0X for un-normalized MTC amplitudes, Σ=1.6X for TPM, Σ=2.2X for internal LTM and Σ=2.0X for external LTM. As for the functional form, three of the four methods appear to give consistent time or frequency dependent responses (see Figure 2), *i.e.* the results from different tracers or cells could be rescaled onto each other by a multiplicative (amplitude) factor. Only the passive MSDs of externally attached tracers showed statistically significant differences in functional form, which will be discussed below. The very large amplitude variation among externally-adhered tracers may be a consequence of variable cell contact areas. Variations in TPM amplitude are presumably due to actual cell to cell response differences. TPM provides an additional control: the two-point correlation function consistently depends on tracer pair separation r as ~1/r, as seen earlier (10). This indicates the response of a three-dimensional network that is essentially homogeneous on the scale of tracer separations studied ($2<r<8$ μm). Given the homogeneity seen by TPM, the large amplitude variation of 4.5 μm diameter internalized tracers, which has been observed previously (11), is somewhat unexpected.

Two Distinct Mechanical Responses. To compare the results of the four methods we compare their frequency dependent shear moduli, normalized by their values at ω=10 rad/sec. The different measurements fall on two distinct 'master'curves, Figure 3. Which response is observed appears to be determined by which region in the cell is being probed. Not surprisingly, LTM with phagocytosed tracers agrees well with the TPM method—both are clearly intracellular—and extends the measured modulus to significantly higher frequency.

Both curves have a weak power-law response at low frequencies crossing over to a nearly $\omega^{3/4}$ regime at high frequency. Indeed, both curves are fit well (Fig 3, dashed lines) by the linear superposition of two power-laws:

$$\begin{aligned} G'(\omega) &= A\cos(\pi\beta/2)\omega^{\beta} + B\cos(3\pi/8)\omega^{3/4} \\ G''(\omega) &= A\sin(\pi\beta/2)\omega^{\beta} + B\sin(3\pi/8)\omega^{3/4} \\ \left|G^*(\omega)\right|^2 &= G'(\omega)^2 + G''(\omega)^2 \end{aligned} \qquad (1)$$

with different values of the parameters *A, B* and β. The upper curve, typified by the TPM measurements, has $\beta_1 = 0.26$, while the lower curve, typified by the results of the MTC experiment, has $\beta_2 = 0.17$, and has a distinctly higher cross-over frequency. The systematic uncertainty in both β values is about 0.02. Allowing the high-frequency exponent to freely vary did not change the quality of fit, and yielded values that were statistically consistent with 0.75.

Interestingly, LTM with externally attached tracers can report either response curve. Roughly 60% of the tracers give results resembling the TPM-like curve, while about 15% of the tracers resemble the MTC-like curve. The remaining data resemble either master curve, but cross over to a purely viscous response at high frequency, which we hypothesize could be due to flexibility in the molecular linkage between the tracer and

cell. Stated another way, the majority of externally attached tracers report distinctly different shear moduli under driving by an external torque and driving by Brownian motion. Deformation fields due to Brownian translational motion should resemble those of tangential point forces, with a long-range decay of form 1/r, while the strain field from torque-induced rocking should resemble normal force dipoles and is expected to decay roughly as $1/r^3$. Indeed, finite element simulations have show the strain field generated by MTC decays by 50% within 500 nm of the surface (12), further suggesting that MTC is a 'shallow' probe of cell mechanics. Overall, our results are most simply explained by two distinct mechanical structures in the cell: one located relatively near the cell surface and the other filling the interior.

Two responses describe available literature data. It appears that both the form in Eq. (1) and the exponent values we have observed are consistent with the results of a large number of earlier studies, some of which have also reported weak power-law or $\omega^{3/4}$ frequency dependences. To facilitate comparison, we compiled dynamic shear moduli, or converted other literature results (such as creep responses) and compare their normalized frequency dependences in Figure 4. Remarkably, the data can be partitioned into two groups, which correspond closely to our two master curves. Not surprisingly, the two reports that match our intracellular response also use large, translating probes (13) or stretch the entire cell uniaxially (14), and have β values of 0.29 and 0.26 respectively, close to our intracellular β_1 value. Literature results using AFM (15), laser tracking (6), magnetic twisting creep (16), MTC (8) and optical tweezers (17) resemble our MTC-like curve, and have β values in the range 0.16-0.18, corresponding to our β_2 value.

A particularly illustrative case is that of Yamada *et al.* (6), which used COS7 cells which are closely related to our TC7 cells. Interestingly, results of their LTM

measurements on small, *intracellular* tracers in cell lamellae closely match our MTC-like master curve (Fig. 4). This appears to rule out the possibility that MTC is measuring the properties of the adhesion complex or ligand contacts. Instead, it suggests that MTC probes a mechanically distinct cell cortex and that this cortical structure forms the predominant part of thin cell processes such as lamellae. LTM data for non-lamellar tracers in the same study appear roughly consistent with our TPM curve. Overall, the agreement of their data with ours suggests that tracers as small as 0.5 μm can yield shear moduli with reliable frequency dependences, provided they are not being affected by molecular motors.

It appears that having two distinct structures, both with weak power-law frequency responses, is a generic feature of many mammalian cell types. Moreover, the close correspondence of our passive methods in ATP depleted cells to these measurements in normal cells underscores the validity of our ATP depletion approach. The remarkably similar response of such a variety of cell types, epithelial (6, 15), endothelial (13), smooth muscle (8, 16) and skeletal myoblasts (14, 17), is somewhat surprising, but is further motivated by the similarity of TPM (10) and MTC (8) measurements of other cell types. It should be noted, however, that our interpretation of literature results does not always agree with that of the study authors, nor does it explain all observations. For example, recent MTC studies find β varies with tracer ligand density and chemistry (18) and an intermediate exponent value (β=0.20) in one cell type (19).

In stark contrast to the remarkable agreement between the frequency dependence of different cell rheology methods, the inferred amplitudes in the literature vary by two orders of magnitude, from tens of Pa to a few kPa (6). As mentioned before, converting any microrheology data to a quantitative stiffness requires modeling. While we do not

resolve the stiffness discrepancies here, TPM does provide a model-independent stiffness. The mean TPM response for ATP depleted cells at a frequency ω =10 rad/sec is $|G^*(\omega)|$ = 38 Pa, with a cell-to-cell standard deviation of Σ=1.6X, *i.e.* most responses fell in the range 20-60 Pa.

Passive microrheology in normal cells confounded by ATP dependent processes. There are many mechanisms other than Brownian fluctuations that can move intracellular particles. Intracellular trafficking by molecular motors can lead to either directed or random motion inside the cell. Cell crawling can cause spurious tracer motion. Reaction forces from trafficking, cytoskeletal treadmilling or remodeling can 'jiggle' the network, also moving tracers. All these processes require metabolic energy. Since energy dissipation increases with velocity, short lag time motion is likely to be Brownian, and non-Brownian effects will dominate at long times.

Typical microrheology data for our three passive methods, both with and without ATP depletion are compared in Fig. 5. For the shortest lag times, there is little change in any of the observed MSDs, consistent with both thermal driving at short lag times and little change in the frequency dependence of the mechanical response. The long-time super-diffusive behavior ($\sim\tau^{\alpha}$, $\alpha>1$) is mathematically inconsistent with the GSER, Eq. 2, underscoring its non-Brownian origin. The super-diffusive results for LTM experiments (Fig. 5A,B) show non-Brownian motion with variable cross-over times and exponents, α. For TPM measurements (Fig. 5C), the non-thermal motion appears at shorter lag times (τ > 3 msec) and is more reproducible in form, with $\alpha\sim1.5$. In an earlier paper (10), we modeled similar long-time data in terms of stress fluctuations driven by random force 'steps' inside a continuum with weak power-law shear modulus $G^*\sim\omega^{\beta}$; predicting a super-diffusive behavior MSD$\sim\tau^{(1+2\beta)}$. The observed super-diffusive exponent is

consistent with $(1+2\beta_l)$, providing a further check that the frequency dependence observed by TPM does not change significantly with ATP depletion.

Lastly, we turn to the amplitude of the shear modulus, rather than its frequency dependence, and whether it changes with ATP depletion, Figure 5D. Given the large amplitude of non-Brownian motion, using TPM we can only sensibly estimate the modulus of normal cells at our highest available frequency, ω= 1000 rad/sec. These cells yield a value of 160 Pa, while TPM of ATP depleted cells yields a value of 217 Pa, which is not a statistically significant change (p=0.17), even when the results of 27 measurements are averaged. These results suggest that any change in stiffness in our TC7 cells due to ATP depletion is modest or non-existent. In contrast, LTM of internalized tracers (assuming Stokes boundary conditions) reports values of 40 Pa (control) and 18 Pa (ATP depleted) at the same frequency, which is a significant change (p=0.003). Since TPM is insensitive to tracer/network coupling, while LTM is not, a natural explanation is that this apparent change with ATP depletion is artifactual, due to ATP depletion induced changes to the tracer/network coupling. The difference between LTM and TPM is both large and highly significant (ATP depleted, $p<10^{-4}$; control, $p<10^{-4}$). As stated above, getting an absolute stiffness figure from LTM requires a model, here a Stokes-like boundary condition. The factor of 4-10X amplitude difference between LTM and TPM indicates that the Stokes model for LTM measurements is not quantitatively accurate. This finding agrees with published results (11) that show the deformation field around similar internalized tracers is much more localized spatially than predicted by the Stokes model.

Discussion

A two-network consensus mechanical response The most significant result of this work is the observation of two distinct viscoelastic cellular mechanical responses, which are both well represented by a simple power-law form (Fig. 2). On the basis of our own data and comparisons with the literature (particularly Yamada (6)), we conclude this phenomenon is caused by two networks in spatially separate compartments corresponding to the cortical/lamellar and deep intracellular space. Moreover, the literature shows (Fig. 4) that a wide variety of mammalian cell types probed with several different techniques give results corresponding to one or the other frequency dependence, suggesting that ours may be a useful consensus description. Since the concentration, organization and types of cytoskeletal polymers are expected to vary amongst cell types, the apparent universality of the responses is somewhat surprising. This suggests either the strong conservation of mechanical properties (e.g. due their criticality for proper cell function) or a generic physical description that allows networks with different structural protein species or concentrations to naturally have such similar mechanics. Lastly, the presence of at least two networks with qualitatively similar responses indicates that researchers must be very careful to test that different tracers are reporting comparable responses prior to pooling multi-tracer results into an ensemble average. For example, external LTM measurements on *Dictyostelium* also display two distinct classes of tracer behavior (20), as we found in mammalian cells.

Unlike the consensus above regarding the frequency dependence and compartmented nature of the mechanical response, there appears to be little agreement on the absolute stiffness of either structure. While some of this discrepancy may reflect real cell type differences in stiffness (without corresponding differences in frequency dependence), it seems more likely to be due to errors in modeling the cytoskeletal

deformation field and structure near tracer probes. Perhaps counter-intuitively, reliably measuring cells' absolute stiffness at a single frequency is more difficult than measuring the frequency dependence of its viscoelastic response. Clearly more work is needed to resolve these issues. TPM does have the advantage of providing a model-independent stiffness value, but only for the interior network and then only in ATP depleted cells. Most cells fall in the range 20-60 Pa, on the low end of literature estimates. Given our finding that ATP depletion has little apparent effect on the mechanical response, it seems likely that untreated normal cells have comparable intracellular stiffness. This finding may be somewhat surprising given the expected biological ramifications of this treatment (disturbed ion homeostasis, myosin bonds going into rigor and eventual depolymerization of the actin cytoskeleton). The seeming independence of cell rheology to these effects will be investigated further in future studies using specific cytoskeletal disruptors and motor inhibitors. Lastly, our work confirms the expectation that non-Brownian, ATP-dependent processes significantly confound passive microrheology methods, limiting their utility in normal cells to high frequencies.

Possible Physical Origins of Cellular Mechanical Response

Over the last few decades, several conceptual models of the cytoskeleton have been proposed to explain different cell mechanical phenomena. The 'sol-gel' model conforms to the conventional notion that the cytoskeleton's mechanical response is due to a 'gel' of filamentary polymers pervaded by a fluid cytosol (21). The 'tensegrity' model seeks to explain experiments indicating that cell stiffness is roughly proportional to intracellular stress (22). Most recently, the Soft Glassy Rheology (SGR) model (23) has been proposed to explain cells' weak power-law rheology (8).

The major theoretical challenge for the cell mechanics field is to develop a model that simultaneously accounts for *all* the cell phenomena and known cell physiology, i.e. one that displays a stress-dependent stiffness, weak power-law rheology and is consistent with cell ultrastructure. By this standard, the existing models appear inadequate. Counter to the early idea that the cytoskeleton is 'simply a gel,' no synthetic material has been found that simultaneously displays cell-like stress-induced stiffening and power-law rheology. The tensegrity model, corresponding to a macroscopic network of opposed elastic struts in tension and compression, does not naturally predict power-law rheology (24). The SGR model, while it neatly explains the power-law response, does not capture stress-induced stiffening. SGR materials, such as foam and toothpaste, generally yield and flow above a critical stress (25), the opposite of the cellular response (26).

Theory aside, researchers have sought a 'minimal in vitro cytoskeleton' that reproduces the cell mechanical response with purified cytoskeletal proteins or to identify synthetic 'model' materials with broadly similar mechanical behavior. Solutions of entangled actin filaments (7) and actin gels cross-linked with simple, irreversible cross-links (27) have a frequency independent elastic response at low frequencies. In contrast, F-actin networks with the protein cross-links α-actinin (28) and filamin A (29) display a more cell-like weak power-law rheology, indicating that these networks undergo structural changes that relax stress on long time-scales. Of these two systems, only the filamin/actin networks also stiffen in response to deformation (30), making them the only material, to our knowledge, to simultaneously show both power-law rheology and cytoskeleton-like stiffening. The filamin/actin gel is not a perfect model, however, as its power-law exponent, β, of about 0.10, is significantly lower than found in either cellular network. On the other hand, these experiments suggest that generically, filamentary network gels with protein cross-links *can* both stiffen in response to stress and have power-law rheology. Future experiments using different cross-links (and perhaps

different filaments) may well produce in vitro gels that replicate the essential features of cytoskeletal mechanics.

The origin of the power-law rheology in these biopolymer gels is currently unknown. It does not seem to resemble synthetic materials having power-law rheology, which can be divided into two classes: SGR materials and critical gels. Unlike SGR materials (23), the in vitro gels do not flow under stress (29), nor do they consist of particles densely crowded together. In critical gels, the power-law response is due to either a scale-free fractal structure (physical gels) (31) or a power-law molecular weight distribution for its constituents (chemical gels) (32). The fractal gels are generally very fragile, unlike the biopolymer gel. Moreover, as chemical critical gels are based on a percolation phenomenon, their behavior is very sensitive to changes in cross-linker concentration, while the biopolymer gel's behavior was not (30).

Power-law rheology implies that the microscopic processes responsible for stress relaxation in a material have a broad distribution of characteristic times (or activation rates). A long-standing idea in the cell mechanics field is that such stress relaxation could be due to discrete unbinding events between or conformational changes in structural proteins (33-35). While we can imagine that the broad distribution of rates in cells is due to a variety of polymer species, the biopolymer gel studies indicate that a single cross-link species can generate power-law rheology. Presumably the distribution of activation rates relates to heterogeneity of the network structure, molecular aggregation/bundling or a distribution of internal stresses. In a recent numerical study (36), we examined the rheology of simplified networks with cross-links that display force-activated serial domain unfolding (4) or unbinding. Under deformation, networks with unfolding domains evolved to an unusual state where many cross-links had near critical forces, allowing thermal activation to unfold them, and leading to power-law

rheology. We further speculated that this arrangement, with many molecules organized on the cusp of a conformational change, is well-suited to act as a biochemical sensor of network deformation. While more detailed simulations and in vitro experiments need to be undertaken, these results suggest that relatively simple polymer physics-based models may be able to explain the observed cell mechanical response and suggest mechanisms for mechano-sensing (5, 37).

Our mechanical measurements on cultured cells suggest a surprisingly universal consensus mechanical response consisting of two regions with similar but quantitatively distinct power-law rheology at low frequencies. Our results underscore the utility of using multiple cell rheology methods in conjunction. This approach should facilitate the quantitative interpretation of future studies, including those that dissect the mechanical responses' molecular determinants using pharmacological and genetic methods.

Methods

Cell culture and ATP depletion. Cells were cultured using Dulbeco's Modified Eagle's Medium (Gibco) supplemented with 10% Bovine Calf Serum (Hyclone), 50mg/ml Gentamicin (Sigma) and penicillin-streptomycin (75 I.U./ml and 75μg/ml) solution (ATCC), at 37 ˚C and 5% CO_2. Cells were transferred to petri-dishes with glass cover-slip bottoms, coated with collagen I (BD BioCoat), and incubated overnight prior to experiments. On an inverted optical microscope (Leica, DM-IRB), the stage, oil-immersion condenser, and 100X NA=1.4, oil-immersion objective were heated to 37˚C and the atmosphere above the cells was maintained at 5% CO_2. Cell viability for up to 8 hours on the microscope was confirmed.

For ATP depletion experiments, the medium was exchanged for serum- and glucose-free Dulbeco's Minimum Essential Medium (Gibco) with 0.05% sodium azide (Alfa Aesar) and 50 mM 2-D-deoxyglucose (Sigma) 1-2 hours prior to data collection. Depletion was verified with a luciferased-based assay (Promega) and showed 98% reduction of ATP. MTC and LTM tracers were attached or internalized prior to ATP depletion. Visualization of F-actin showed no noticeable change to the density or distribution of F-actin upon ATP depletion, other than a slight reduction in the number of stress fibers.

MTC and LTM. Measurements used ferromagnetic beads (4.5μm diameter, Spherotech) coated with RGD-peptide (Integra-LS), attached to the cell exterior via integrin receptors, or phagocytosed into the cell interior. For MTC, beads were magnetized vertically after cell attachment using a ~1000 Gauss magnetic field pulse lasting ~100 μsec. Beads were selected visually in bright-field; cells with multiple beads were rejected. Tracers were illuminated with a red laser diode (λ=638 nm), keeping absorbed laser power < 1/3 mW to minimize heating effects (estimated to be about 1°C/mW) and imaged on a quadrant

photodiode (Centrovision) with a 4.5x auxiliary magnification and dark-field Fourier filter. Bead displacement resolution is ~ 0.2 nm for lag times <100μsec (shot noise limited) and ~1 nm for lag times >10msec (vibration limited).

In MTC experiments, externally attached beads were rocked by a 10 Gauss (peak) oscillatory horizontal magnetic field. The magnet current and bead-position signals were simultaneously digitized at 50 kHz (National Instruments). The amplitude and phase shift of the bead displacement were determined in real time using a LabView-based digital lock-in. The displacement amplitude is inversely proportional to the shear modulus at the driving frequency, but also depends on details of the bead-cell contact, which is assumed to contribute a frequency-independent prefactor. To avoid errors due to time-dependence of this prefactor during frequency sweeps, we drive the bead with a sum of two sinusoids, sweeping one and using the other as a reference (at 5 Hz). The ratio of the two amplitudes is nearly time-independent, allowing the more precise determination of the frequency-dependence of G' and G" with single cells.

For passive LTM experiments, no field was applied and the random bead deflection signal was digitized at rates up to 50 kHz. Trajectories were digitally filtered to remove narrow-band vibration signals, and mean square displacements (MSD) computed. At lag times where the motion is predominantly Brownian, G' and G" can be computed from the MSD using the generalized Stokes-Einstein relation (GSER),

$$\left\langle \Delta r^2(\omega) \right\rangle = k_B T / \pi i \omega G^*(\omega) a. \qquad (2)$$

and numerical methods previously described. The same algorithms were used to convert literature MSD or creep compliance data as needed.

TPM and multi-particle tracking. Cells were imaged with shadow-cast DIC microscopy with illumination provided by a pulsed, fiber-scrambled 2W diode laser

(Spectra Diode Labs, SDL-2460, λ = 808 nm). Images were focused 2-4 μm into the 6-10 μm thick TC7 cells. For each cell, ~35,000 images were recorded over a 25 minute period, at rates of 50 and 1000 frames/sec using a digital CMOS camera (Phantom 4, Vision Research). The cell was illuminated with a 20-30 μsec laser strobe and the image scale was 96 nm/pixel. A few hundred ~0.5 μm endogenous particles (presumed by morphology to be primarily lipid granules and mitochondria) were found within each cell and ~2 μm depth of focus, yielding ~10^7 positions per single cell dataset with 5-8 nm spatial resolution. Tracers in nuclei or thin lamellae were omitted. Algorithms for particle tracking (38) and computing two-point correlations (7) are described elsewhere. Briefly, the random motion of each pair of tracers during a lag time τ is decomposed into components along and perpendicular to their line of centers. The parallel components are multiplied together, partitioned in r and averaged to determine a statistical covariance, $D_{rr}(r, \tau)$. The covariance values with $2<r<8$ μm are multiplied by r, further averaged together and rescaled to resemble a mean-squared displacement (MSD). This MSD can be converted to shear moduli (39) as with LTM, above.

Log-normal statistics. Our measurements appear log-normal distributed, meaning that their logarithms are Gaussian distributed. When combining or comparing results from different tracers, we compute the mean, standard deviation and significance tests using log-transformed data. The mean of the log-transformed values is exponentiated to yield the reported average value, M. The standard deviations, σ, of the log-transformed data are exponentiated to yield 'multiplicative' log-normal standard deviations, Σ. For example, values of M=5 and Σ=2X would imply that ~70% of the data (1σ confidence interval) would fall in the range 2.5 – 10 (M/Σ – $M*\Sigma$).

Acknowledgements

This work was supported by the David and Lucile Packard Foundation, Penn's MRSEC and the bourse Lavoisier du Ministère Français des Affaires Etrangères. We are grateful to K. Dahl, D. Discher, J.J. Fredberg, M. Gardel, D. Hammer, P. Janmey, S. Kuo, I. Levitan, V. Weaver and D. Weitz for useful discussions, and to W. Feneberg for providing published data.

References

1. McBeath, R., Pirone, D. M., Nelson, C. M., Bhadriraju, K. & Chen, C. S. (2004) *Dev Cell* **6,** 483-95.
2. Paszek, M. & Weaver, V. (2004) *J Mammary Gland Bio and Neoplasia* **9,** 325-342.
3. Engler, A. J., Griffin, M. A., Sen, S., Bonnemann, C. G., Sweeney, H. L. & Discher, D. E. (2004) *J Cell Biol* **166,** 877-87.
4. Rief, M., Pascual, J., Saraste, M. & Gaub, H. E. (1999) *J Mol Biol* **286,** 553-61.
5. Janmey, P. A. & Weitz, D. A. (2004) *Trends Biochem Sci* **29,** 364-70.
6. Yamada, S., Wirtz, D. & Kuo, S. C. (2000) *Biophys J* **78,** 1736-47.
7. Crocker, J. C., Valentine, M. T., Weeks, E. R., Gisler, T., Kaplan, P. D., Yodh, A. G. & Weitz, D. A. (2000) *Phys Rev Lett* **85,** 888-91.
8. Fabry, B., Maksym, G. N., Butler, J. P., Glogauer, M., Navajas, D. & Fredberg, J. J. (2001) *Phys Rev Lett* **87,** 148102.
9. Levine, A. J. & Lubensky, T. C. (2000) *Phys Rev Lett* **85,** 1774-7.
10. Lau, A. W., Hoffman, B. D., Davies, A., Crocker, J. C. & Lubensky, T. C. (2003) *Phys Rev Lett* **91,** 198101.
11. Bausch, A. R., Möller, W. & Sackmann, E. (1999) *Biophys J* **76,** 573-579.
12. Mijailovich, S. M., Kojic, M., Zivkovic, M., Fabry, B. & Fredberg, J. J. (2002) *J Appl Physiol* **93,** 1429-36.
13. Feneberg, W., Aepfelbacher, M. & Sackmann, E. (2004) *Biophys J* **87,** 1338-50.
14. Desprat, N., Richert, A., Simeon, J. & Asnacios, A. (2005) *Biophys J* **88,** 2224-33.
15. Alcaraz, J., Buscemi, L., Grabulosa, M., Trepat, X., Fabry, B., Farre, R. & Navajas, D. (2003) *Biophys J* **84,** 2071-9.
16. Lenormand, G., Millet, E., Fabry, B., Butler, J. & Fredberg, J. (2004) *J of the Royal Soc Interface* **1,** 91-97.
17. Balland, M., Richert, A. & Gallet, F. (2005) *Eur Biophys J* **34,** 255-61.
18. Puig-de-Morales, M., Millet, E., Fabry, B., Navajas, D., Wang, N., Butler, J. P. & Fredberg, J. J. (2004) *Am J Physiol Cell Physiol* **287,** C643-54.
19. Laudadio, R. E., Millet, E. J., Fabry, B., An, S. S., Butler, J. P. & Fredberg, J. J. (2005) *Am J Physiol Cell Physiol* **289,** C1388-95.
20. Girard, K. D., Kuo, S. C. & Robinson, D. N. (2006) *Proc Natl Acad Sci U S A* **103,** 2103-8.
21. Janmey, P. A., Hvidt, S., Lamb, J. & Stossel, T. P. (1990) *Nature* **345,** 89-92.
22. Ingber, D. E. (2003) *J Cell Sci* **116,** 1157-73.
23. Sollich, P. (1998) *Phys Rev E* **58,** 738-759.
24. Sultan, C., Stamenovic, D. & Ingber, D. E. (2004) *Ann Biomed Eng* **32,** 520-30.
25. Mason, T. G., Bibette, J. & Weitz, D. A. (1995) *Phys Rev Lett* **75,** 2051-2054.
26. Stamenovic, D., Suki, B., Fabry, B., Wang, N. & Fredberg, J. J. (2004) *J Appl Physiol* **96,** 1600-5.
27. Gardel, M. L., Shin, J. H., MacKintosh, F. C., Mahadevan, L., Matsudaira, P. & Weitz, D. A. (2004) *Science* **304,** 1301-5.
28. Palmer, A., Xu, J., Kuo, S. C. & Wirtz, D. (1999) *Biophys J* **76,** 1063-71.

29. Gardel, M., Nakamura, F., Hartwig, J., Crocker, J., Stossel, T. & Weitz, D. (2006) *Phys Rev Lett* **96,** 188102-(1-4).
30. Gardel, M. L., Nakamura, F., Hartwig, J. H., Crocker, J. C., Stossel, T. P. & Weitz, D. A. (2006) *Proc Natl Acad Sci U S A* **103,** 1762-7.
31. Richtering, H., Gagnon, K., Lenz, R., Fuller, R. & Winter, H. (1992) *Macromolecules* **25,** 2429-2433.
32. Izuka, A., Winter, H. & Hashimoto, T. (1992) *Macromolecules* **25,** 2422-2428.
33. Wachsstock, D. H., Schwarz, W. H. & Pollard, T. D. (1994) *Biophys J* **66,** 801-9.
34. Furuike, S., Ito, T. & Yamazaki, M. (2001) *FEBS Lett* **498,** 72-5.
35. Bausch, A. R., Hellerer, U., Essler, M., Aepfelbacher, M. & Sackmann, E. (2001) *Biophys J* **80,** 2649-57.
36. Hoffman, B., Massiera, G. & Crocker, J. C. (2006) (arXiv preprint, physics/0504051.
37. Vogel, V. & Sheetz, M. (2006) *Nat Rev Mol Cell Bio* **7,** 265-275.
38. Crocker, J. & Grier, D. (1996) *J Colloid Interface Sci* **179,** 298-310.
39. Mason, T. (2000) *Rheologica Acta* **39,** 371-378.

Figure Legends

Fig. 1. Sketch of our four cell rheology techniques. From top to bottom, MTC measures the rocking motion of 4.5 μm diameter tracers, adhered to the apical cell surface by integrins, in response to a sinusoidal magnetic torque. TPM measures the correlation of the random motion of pairs of endogenous tracers to infer the Brownian fluctuations of the intervening network. LTM measures the translational Brownian motion of the MTC tracers either phagocytosed into the cell interior or on the apical surface.

Fig. 2. Typical data from our four methods on ATP-depleted TC7 epithelial cells (curves). (*A*) Shear modulus (normalized such that $|G^*(\omega/2\pi=5\ \text{Hz})| = 1$) reported for ATP-depleted cells (closed symbols) compared to untreated cells (open symbols). (*B*) Mean squared displacement (MSD) reported by TPM, scaled to a 4.5 μm tracer. (*C*) Passive MSD's for phagocytosed 4.5 μm tracers. (*D*) Passive MSD's for external, integrin-adhered 4.5 μm tracers.

Fig. 3. Normalized shear modulus for ATP depleted cells collapse onto two master curves (offset by 2X for clarity). As discussed in the text, the upper curve is the TPM-like response and the lower is the MTC-like response. The small black points are from single tracer external bead LTM trajectories, which can correspond to either curve. The squares are cell-averaged internal (phagocytosed) LTM data (N = 41), triangles a typical single cell MTC response and open circles are cell-averaged TPM (N = 7). Dashed lines are best fits of Eq. 1 to data (upper curve: β_1=0.26, A=0.51, B=0.020; lower curve: β_2=0.17, A=0.66, B=0.009; both normalized at 10 rad/sec). High frequency line has slope 0.75.

Fig. 4. Summary of literature shear moduli versus frequency, offset vertically for clarity. From top to bottom: mechanical measurements from (a) cell creep (magnetic pulling) (13), (b) uniaxial rheometry (14), (c) AFM (15), (d) LTM in the

lamellae (6), (e) cell creep (magnetic bead twisting) (16), (f) MTC (8), and optical tweezers (17). All data are well fit to a sum of power-laws, Eq. 2. Interestingly, magnetic pulling and uniaxial rheometry (a,b) results have fit slopes of 0.29 and 0.26 (comparable to our intracellular curve), while others (c-g) have slope of 0.16-0.18 (comparable to our cortical curve).

Fig. 5. Comparison of ATP depleted (filled symbols) and untreated TC7 cells (open symbols). (*A*) Typical external LTM data for tracers showing typical cortical (upper) and intracellular (lower) responses. The curves are offset by a factor of 4 and aligned at the shortest time point. (*B*) Averaged MSD's for internalized tracers by LTM, N = 23 cells (ATP-), 21 (control, ATP+). (*C*) Averaged MSD's reported by TPM (scaled to a 4.5 μm tracer), N = 7 (ATP-), 20 (control, ATP+) (D) the shear modulus (in Pa) at ω=1000 rad/sec. Error bars are log-normal standard errors.

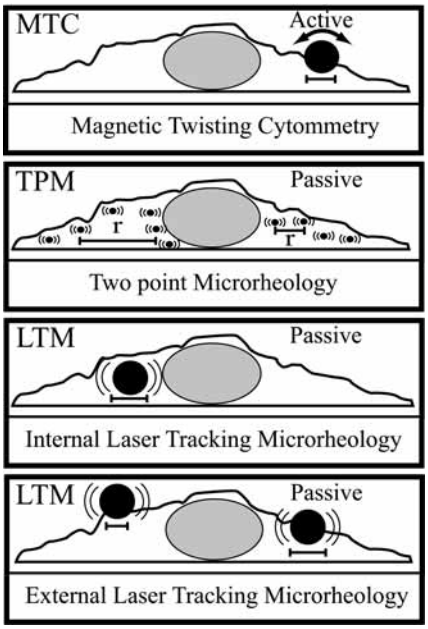
MTC
Active
Magnetic Twisting Cytommetry
TPM
Passive
r
r
Two point Microrheology
LTM
Passive
Internal Laser Tracking Microrheology
LTM
Passive
External Laser Tracking Microrheology

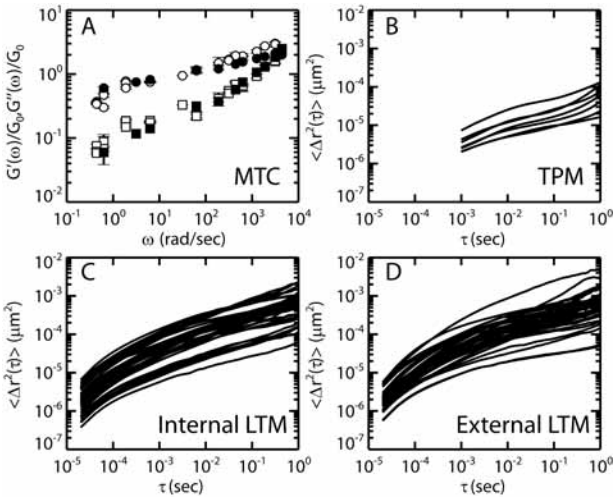
A
MTC
G'(ω)/G0,G''(ω)/G0
ω (rad/sec)
B
TPM
<Δr²(τ)> (μm²)
τ (sec)
C
Internal LTM
D
External LTM

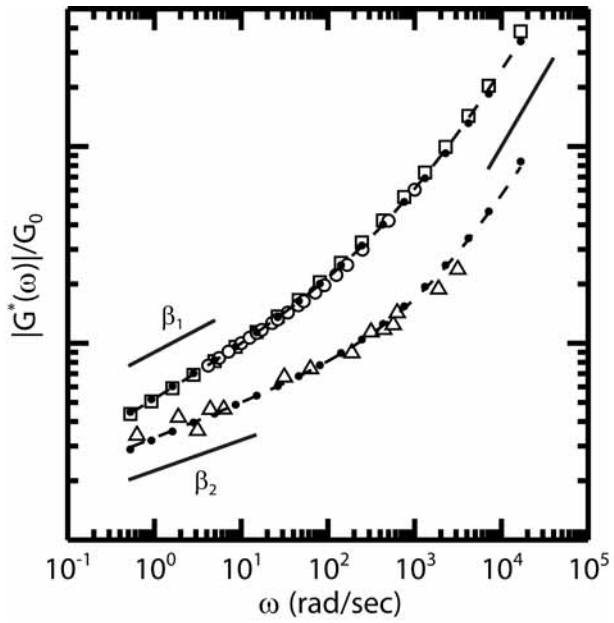
|G*(ω)|/G0
β1
β2
10-1
100
101
102
103
104
105
ω (rad/sec)

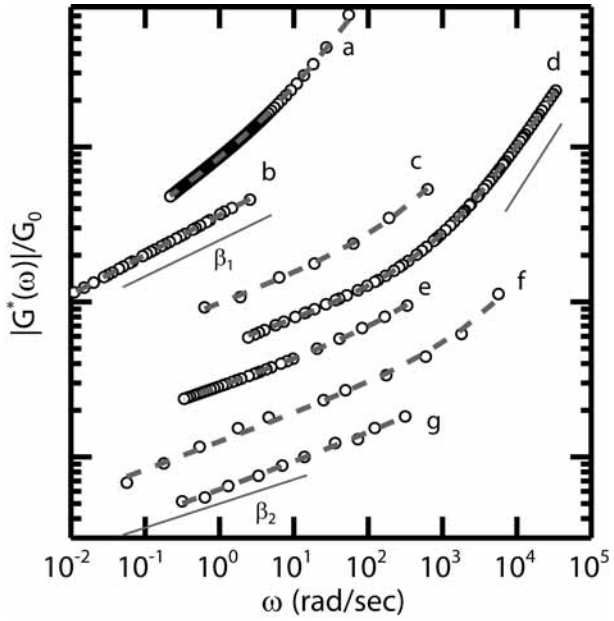
a
b
c
d
e
f
g
β1
β2
|G*(ω)|/G0
10-2 10-1 100 101 102 103 104 105
ω (rad/sec)

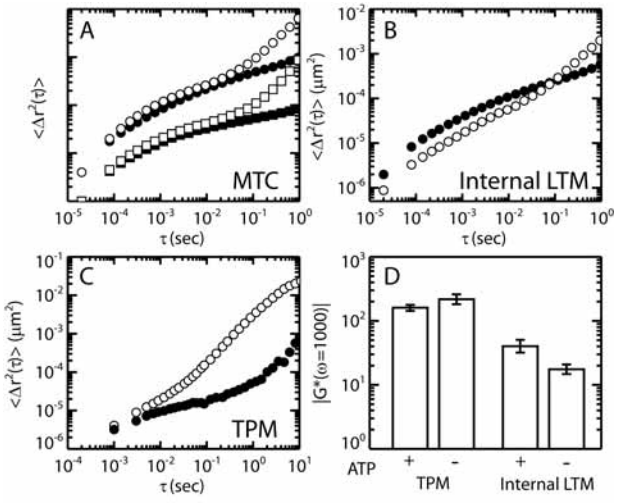
A
MTC
B
Internal LTM
C
TPM
D
τ (sec)
ATP
+
-
TPM
Internal LTM